Analyzing X-Ray Pulsar Profiles: Geometry and Beam Pattern of Her X-1

S. Blum and U. Kraus
Institut für Astronomie und Astrophysik, Abteilung Theoretische Astrophysik,
Universität Tübingen,
Auf der Morgenstelle 10, 72076 Tübingen, Germany

ABSTRACT

We report on our analysis of a large sample of energy dependent pulse profiles of the X-ray binary pulsar Hercules X-1. We find that all data are compatible with the assumption of a slightly distorted magnetic dipole field as sole cause of the asymmetry of the observed pulse profiles. Further the analysis provides evidence that the emission from both poles is equal. We determine an angle $\Theta_{\rm m} < 20^\circ$ between the rotation axis and the local magnetic axis. One pole has an offset $\delta < 5^\circ$ from the antipodal position of the other pole. The beam pattern shows structures that can be interpreted as pencil- and fan-beam configurations. Since no assumptions on the polar emission are made, the results can be compared with various emission models. A comparison of results obtained from pulse profiles of different phases of the 35-day cycle indicates different attenuation of the radiation from the poles being responsible for the change of the pulse shape during the main-on state. These results also suggest the resolution of an ambiguity within a previous analysis of pulse profiles of Cen X-3, leading to a unique result for the beam pattern of this pulsar as well. The analysis of pulse profiles of the short-on state indicates that a large fraction of the radiation cannot be attributed to the direct emission from the poles. We give a consistent explanation of both the evolution of the pulse profile and the spectral changes with the 35-day cycle in terms of a warped precessing accretion disk.

1. Introduction

Since its discovery in 1972 by the UHURU satellite (Tananbaum et al. 1972), the X-ray binary system Hercules X-1/HZ Herculis has become the best studied of its class of about 44 known today (Bildsten et al. 1997). They are understood to be fast spinning neutron stars that are accreting matter from a massive companion star either via Roche lobe overflow or from the stellar wind of the companion. Since the neutron stars have strong magnetic fields, the accreted matter is funnelled along the field lines onto the magnetic poles, where most of the energy is released in form of X-radiation. Generally the magnetic axis and the rotation axis are not aligned. Therefore a large fraction of the detected flux from these sources is pulsed as during the course of each revolution of the neutron star the beams from the poles sweep through our line of sight.

Her X-1/HZ Her combines most of the properties that can be found in X-ray binaries, this made it one of the favourite sources of X-ray astronomers. From the observation of eclipses and from pulse timing analyses the orbital parameters are well determined. The masses of the neutron star and its optical companion are 1.3 $M_\odot$ and 2.2 $M_\odot$ respectively, the orbital period of Her X-1 is 1.7 d, and the inclination of the orbital plane is $i > 80°$ (Deeter, Boynton, & Pravdo 1981). In addition to the pulse period of 1.24 s, i.e. the rotation period of the neutron star, Her X-1 also displays X-ray intensity variations on a period of about 35 days. Such a long-term variability is only known for two other pulsars: LMC X-4 and SMC X-1. The 35-day cycle of Her X-1 is nowadays ascribed to the precession of a warped accretion disk which periodically obscures the neutron star from our view (Petterson, Rothschild, & Gruber 1991, Schandl & Meyer 1994). During its high intensity or main-on state, Her X-1 has a luminosity $L_{\rm x} \approx 2.5 \cdot 10^{37}$ ergs s^{-1} (2-60 keV) (McCray et al. 1982). The maximum flux of the short-on state is typically only 30% of that of the main-on. Balloon observations in 1977 allowed for the first time the indirect measurement of the magnetic field strength of some 10^{12} G by the revelation of a spectral feature in the hard X-ray spectrum (Trümper et al. 1978), interpreted as a cyclotron absorption line at about 40 keV.

The pulse shapes of Her X-1 are highly asymmetric and depend on energy and on the phase of the 35-day cycle. In several studies phenomenological emission patterns have been used to reproduce the asymmetric pulse profiles of Her X-1. Wang & Welter (1981) fitted the geometry of two antipodal polar caps with asymmetric fan-beam patterns. In this approach the asymmetry of the emission pattern was attributed to asymmetric accretion due to the plasma becoming attached to the magnetic field lines away from the corotation radius. However it is not clear whether an asymmetric accretion stream must produce an asymmetric beam pattern (Basko & Sunyaev 1975). Another way of introducing asymmetry into the pulse shapes is via non antipodal emission regions. Leahy (1991) used two offset rings on the surface of the neutron star with symmetric pencil-beams and Panchenko & Postnov (1994) modelled two antipodal polar caps and one ringlike area which was attributed to a non-coaxial quadrupole configuration of the magnetic field. Further studies have shown that relativistic light deflection near the neutron star plays an important role when emission models are used to explain the observed pulse shapes (e.g. Riffert et al. 1993, Leahy & Li 1995).

In this analysis we take up the idea of a non antipodal location of the emission regions caused by a slightly distorted magnetic dipole field. We assume that the emission originating from the regions near the magnetic poles only depends on the viewing angle between the magnetic axis and the direction of observation which means that the emission is symmetric with respect to the local magnetic axis. In contrast to previous studies where specific emission models have been used to fit the pulse profiles, the method used here does not involve any assumptions on the polar emission. Instead it tests in a general way whether the pulse profiles are compatible with the assumption that they are the sum of two independent symmetric components.

The method we use to analyze pulse profiles is briefly summarized in the following §2.1. In

§2.2 we list the analyzed data. The results of the analysis are presented in §2.3. We show that the data of Her X-1 are indeed compatible with the idea of a slightly distorted magnetic dipole field. Further we find indications in the contributions to the pulse profiles that the emission from both poles is identical. We determine the location of the magnetic poles and reconstruct the beam pattern, which is discussed in §3.1. In the following §3.2 we examine the dependence of the pulse shape on the phase of the 35-day cycle. We argue that the contributions to the pulse profile undergo different attenuation resulting in the observed evolution of the pulse shapes during the main-on state of the 35-day cycle.

2. Analysis

2.1. The Method

This section is a short summary of the method we use to analyze the energy dependent pulse profiles of Her X-1. We will focus on the main ideas and assumptions omitting both formal derivations and technical details. A comprehensive presentation of the material including a test case has been given in Kraus et al. (1995).

Consider the emission region near one of the magnetic poles of the neutron star. Radiation escapes from the accretion stream and from the star's surface and, while close to the star, is deflected in the gravitational field of the neutron star. A distant observer who cannot spatially resolve the emission region measures the integrated flux coming from the entire visible part of the emission region. The observed integrated flux depends on the direction of observation because the direction of observation determines which part of the emission region is visible and also because the radiation emitted by the accretion stream and the neutron star is presumably beamed. This function, namely the flux of a single emission region measured by a distant observer as a function of the direction of observation, is the link between the properties of the emission region and the contribution of that emission region to the pulse profile. In the following we will call this function the beam pattern of the emission region. The contribution of the emission region to the pulse profile, which we will refer to as a single-pole pulse profile, depends both on the beam pattern and on the pulsar geometry, i.e., on the orientation of the rotation axis with respect to the direction of observation and on the location of the magnetic pole on the neutron star. In short: local emission pattern plus relativistic light deflection determine the beam pattern, beam pattern plus geometry result in a certain single-pole pulse profile and the superposition of the single-pole pulse profiles of the both emission regions is the total pulse profile.

a. decomposition into single-pole pulse profiles

In the following we are going to assume that the beam pattern is axisymmetric with respect to the magnetic axis (i.e., to the axis that passes through the center of the neutron star and through the magnetic pole). The axisymmetric beam pattern is a function of only one variable, the angle θ between the direction of observation and the magnetic axis. Consider now the single-pole pulse profile $f(\phi)$, where ϕ is the angle of rotation of the neutron star. It can easily be shown that the single-pole pulse profile produced by an axisymmetric beam pattern is symmetric in the following sense: there is a rotation angle Φ, so that $f(\Phi - \phi) = f(\Phi + \phi)$ for all values of ϕ. The fact that f is periodic in ϕ implies that the same symmetry must hold with respect to the rotation angle $\Phi + \pi$.

Now turn to the total pulse profile produced as the sum of the two symmetric single-pole pulse profiles. If the emission regions are antipodal, i.e., the two magnetic axes are aligned, it turns out that the symmetry points Φ_1 and $\Phi_1 + \pi$ of the first single-pole pulse profile fall on the same rotation angles as the symmetry points Φ_2 and $\Phi_2 + \pi$ of the second single-pole pulse profile. Their sum, the total pulse profile, is therefore symmetric with respect to the same symmetry points. If the emission regions are not antipodal, however, the symmetry points of the two single-pole pulse profiles do not coincide (except for certain special displacements from the antipodal positions) and the total pulse profile is asymmetric.

Given an observed asymmetric pulse profile, we can ask if it could possibly have been built up out of two symmetric contributions with symmetry points that do not coincide. If so, it must be possible to find two symmetric (and periodic) functions f_1 and f_2 with the pulse profile f as their sum. By writing the observed pulse profile, defined by a certain number N of discrete data points $f(\phi_k)$, as a Fourier sum and with an ansatz for f_1 and f_2 in the form of Fourier sums also, the following can easily be shown: For an arbitrary choice of symmetry points Φ_1 and Φ_2, there are two periodic functions f_1 and f_2, f_1 symmetric with respect to Φ_1 and f_2 symmetric with respect to Φ_2, such that $f = f_1 + f_2$, and the two symmetric functions are uniquely determined. Exceptions to this rule occur only if $(\Phi_1 - \Phi_2)/\pi$ is a rational number. In this case the symmetric functions may not exist or, if they exist, may not be uniquely determined. It must also be noted that the symmetric functions obviously can only be determined up to a constant C, since $f_1 + C$ and $f_2 - C$ are also a solution if f_1 and f_2 are.

Thus, in principle every choice of a pair of symmetry points corresponds to a unique decomposition of any pulse profile into two symmetric contributions. For such a decomposition to be an acceptable solution, however, f_1 and f_2 also have to meet the following physical criteria in order to be interpreted as single-pole pulse profiles:

1. They must not have negative values, since they represent photon fluxes.
2. They must be reasonably simple and smooth. We do not expect the polar contributons to have a shape that is more complex than the pulse profile. Especially modulations of the

single-pole pulse profiles that cancel out in the sum are not compatible with the assumption of two independent and therefore uncorrelated emission regions.

3. They must conform to the energy dependence of the pulse profile. The decomposition can be done independently for pulse profiles in different energy ranges. Since the symmetry points are determined by the pulsar geometry, the same symmetry points must give acceptable decompositions according to the criteria 1 and 2 in all energy ranges. Finally the single-pole pulse profiles should show the same gradual energy dependence as the pulse profile.

Given the existence of formal decompositions for all pairs of symmetry points and the criteria mentioned above, we are left with the two-dimensional parameter space of all possible values of Φ_1 and Φ_2, which we search for points with acceptable decompositions. For practical purposes, the parameters we use are the quantities Φ_1 and $\Delta := \pi - (\Phi_1 - \Phi_2)$. The parameter space that contains every possible unique decomposition then is $0 \leq \Phi_1 \leq \pi$ and $0 \leq \Delta \leq \pi/2$. In the analysis of just one pulse profile there will in general be a number of different acceptable decompositions. This number may be significantly reduced by the energy dependence of the pulse profile. In general, the existence of symmetry points with acceptable decompositions in all energy channels is by no means guaranteed. If such a pair of symmetry points is found, then it is indeed possible to build up the observed pulse profile out of two symmetric contributions, and we can conclude that the analyzed data are compatible with the assumption that the asymmetry of the observed pulse profile is caused by the non-antipodal locations of the magnetic poles. The symmetric functions can be interpreted as the single-pole pulse profiles due to the two emission regions.

A successful decomposition provides information both on the geometry and on the beam pattern. As to the geometry, we obtain a value for the parameter Δ. This parameter is related to the locations of the emission regions on the neutron star (see Figure 1). The beam pattern is related to the single-pole pulse profile via the geometric parameters, i.e., the location of the emission region on the neutron star and the direction of observation. Since these parameters are not known, one cannot directly deduce the beam pattern from the single-pole pulse profile. It can be shown, however, that an appropriate transformation of the single-pole pulse profile and the beam pattern turns the transformed single-pole pulse profile into a scaled, but undistorted copy of a section of the transformed beam pattern. Although the scaling factor is a geometric quantity and therefore not known, this still provides an intuitive understanding of what a section of the beam pattern must look like. Since in the case of Her X-1 it is possible to eventually reconstruct the beam pattern, the information obtained at this stage mainly serves as a starting point for the next step of the analysis and we will not go into details about the transformation mentioned above.

b. search for an overlap region and determination of the geometry

In general, the two emission regions on the neutron star may or may not be equal (i.e., have the same beam pattern). If they are equal, this fact may be apparent in the single-pole pulse profiles in the following way. Since in general the rotation axis and the magnetic axis of the neutron star are not aligned, the viewing angle θ between the magnetic axis and the direction of observation of each emission region changes with rotation angle ϕ. The range θ can cover for each magnetic pole depends on the location of that pole on the neutron star and on the direction of observation, where $0^\circ \leq \theta_{\min} \leq \theta_{\max} \leq 180^\circ$. Only in the special case where both the magnetic axis and the direction of observation are perpendicular to the rotation axis, θ takes all values between 0° and 180°. Since the emission regions have different locations on the neutron star, their ranges of values of θ are different. Depending on the geometry, these two ranges for θ may overlap. For an ideal dipole configuration e.g., the condition under which an overlap in the ranges of values of θ of the both poles exists is $\Theta_{\rm O} + \Theta_{\rm m} > \pi/2$, where $\Theta_{\rm O}$ is the angle between the rotation axis and the line of sight, and $\Theta_{\rm m}$ is the angle between the rotation axis and the magnetic axis. Consider an angle $\tilde{\theta}$ in the overlap region. At some instant during the course of one revolution of the neutron, at rotation angle ϕ, one emission region is seen under the angle $\tilde{\theta}$. At a different instant, at rotation angle ϕ', the other emission region is seen under the same angle $\tilde{\theta}$. If the beam patterns of the two emission regions are identical, then the flux detected from the one emission region at ϕ is equal to the flux detected from the other emission region at ϕ'. Thus, if an overlap region exists, the corresponding part of the beam pattern shows up in both single-pole pulse profiles, though at different values of rotation angle. Since the single-pole pulse profiles can be transformed into undistorted (though scaled) copies of sections of the beam patterns, such a part of the beam pattern that shows up in both single-pole pulse profiles should be readily recognizable. Note that the occurence and size of the overlap region depends on the geometric parameters and must therefore be the same for pulse profiles in different energy channels.

If an overlap region is found in the single-pole pulse profiles obtained in the decomposition, this is an indication that there are two emission regions with identical beam patterns. Since each single-pole pulse profile provides a section of the beam pattern and the two sections overlap, we can then combine the two sections by superposing the overlapping parts. As a result we obtain the total visible section of the beam pattern. Superposing the overlapping parts of the two sections of the beam pattern amounts to determining the relation between the corresponding values ϕ and ϕ' of the rotation angle. On the other hand, the relation between ϕ and ϕ' can be expressed in terms of the unknown geometric parameters of the system. Thus, the superposition provides a constraint on the geometry.

Again omitting all details we simply note the procedure for superposing the overlapping parts of the two sections of the beam pattern. The single-pole pulse profiles $f_1(\phi)$ with symmetry point Φ_1 and $f_2(\phi)$ with symmetry point Φ_2 are transformed into functions of a common variable q through $\cos(\phi - \Phi_1) = q$ for f_1 and $\cos(\phi - \Phi_2) = (q - a)/b$ for f_2. The real numbers a and $b > 0$ are determined by means of a fit which minimizes the quadratic deviation between $f_1(q)$

and $f_2(q)$ in the overlap region. At this point the constant C, which determines how the unpulsed flux has to be distributed to the single-pole pulse profiles, can also be computed. Since a and b can be expressed in terms of the unknown geometric parameters of the pulsar, their best-fit values constitute constraints on the pulsar geometry. The results of this second step of the analysis are the total visible beam pattern as a function of q and two constraints on the geometric parameters.

The geometric information obtained so far (i.e., the values of Δ, a, and b) is not quite sufficient in itself to completely determine the pulsar geometry. It needs to be supplemented by an independent determination of any one additional geometric parameter or by an additional constraint. We suggest that this supplement may be obtained by means of the assumption that the rotation axis of the neutron star is perpendicular to the orbital plane. In this case, the angle Θ_O between the direction of observation and the rotation axis of the neutron star is given by the inclination of the orbital plane. The assumption of $\Theta_O = i$ seems to be quite plausible since accreted mass also carries angular momentum from the massive companion, and this transfer is expected to align the rotation axes of the binary stars on a timescale short compared to the lifetime of the system. However, this assumption must not hold true for all binary systems. With the inclination substituted for Θ_O, the analysis of the pulse profiles determines the positions of the emission regions on the neutron star.

Once the pulsar geometry is known, we also obtain the equation relating the auxiliary variable q and the viewing angle θ, so that the reconstructed beam pattern can be transformed into a function of θ. However, it turns out that the relation between q and θ involves an ambiguity which cannot be resolved within this analysis. It is due to the fact that we are not able to relate a single-pole pulse profile to one of the two emission regions. Therefore, we obtain two different possible solutions for the beam pattern and a choice between them must be based on either theoretical considerations and model calculations, or on additional information on the source.

2.2. The Data

The analysis presented in this paper is based on pulse profiles of the main-on and short-on states of Her X-1. The analyzed sample contains a total of 148 pulse profiles from 20 different observations. References, the platform of the detectors, year of observation, the total energy range, the state of the 35-day cycle, the number of separate observations and the total number of pulse profiles of the respective observations are listed in Table 1. The data reduction including background subtraction has been done by the respective authors. In order to compare the pulse profiles from different observations, the pulse profiles of the main-on have been aligned in phase so that their common features match best. Since the pulse profiles of the short-on are markedly different, their features have been aligned with respect to the main-on as suggested by Deeter et al. (1998).

At energies below 1 keV, the pulses of Her X-1 have a sinusoidal shape which is interpreted

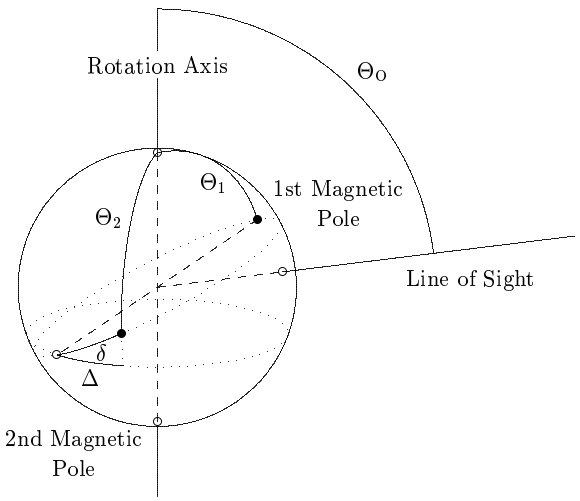

Fig. 1.— *Intrinsic pulsar geometry: the locations of the magnetic poles on the neutron star surface can be described by means of their polar angles* Θ_1 *and* Θ_2 *with respect to the rotation axis and by the angular distance* δ *between the location of one magnetic pole and the point that is antipodal to the other magnetic pole.*

Table 1. Analyzed Data

Reference	Instr. Platform	Year of Obs.	Energy Range (keV)	35-Day State	No. of Obs.[a]	Pulse Profiles[b]
Kuster et al. 1998	RXTE	1997	2 - 19	turn-on	1	25
Soong et al. 1990a	HEAO-1	1978	12 - 55	main-on	1[c]	5
Kahabka 1987	EXOSAT	1984/1985	0.9 - 29	main-on	4	48
Kunz 1996[d]	Kvant	1987/1988	16 - 30	main-on	1[c]	1
Scott 1993	Ginga	1988-1990	1 - 37	main-on	8	40
Stelzer 1997[d]	RXTE	1996	2 - 26	main-on	1	9
Kahabka 1987	EXOSAT	1984	0.9 - 23	short-on	1	11
Scott 1993	Ginga	1989	1 - 14	short-on	3	9

[a]Number of separate observations

[b]Total number of pulse profiles in different energy subranges

[c]Several pointings have been integrated

[d]private communication

as reprocessed hard X-radiation at the inner edge of the accretion disk (McCray et al. 1982). Since the origin of these soft X-rays is not the region near the magnetic poles, the analysis is restricted to higher energies. Above 1 keV the pulse profiles of Her X-1 are highly asymmetric and their typical energy dependence has been examined in a variety of studies (see Deeter et al. 1998, and references therein). In the analysis the pulse profiles are written as Fourier series. Since the higher Fourier coefficients are presumably affected by aliasing and also may have fairly large statistical errors, the highest coefficients are set to zero. This has a smoothing effect depending on the number of Fourier coefficients concerned. An example of the typical energy dependence of the pulse profiles and their representation in the analysis is given in the top row of Figure 2. It shows pulse profiles in three different energy ranges of an EXOSAT observation (Kahabka 1987) during the main-on state. The observed pulse profiles are plotted with crosses. The profiles plotted as solid lines are inverse Fourier-transformed using 32 out of originally 60 Fourier coefficients.

2.3. Results

a. decomposition into single-pole pulse profiles

In a first run, the decomposition method has been simultaneously applied to the 103 pulse profiles of the 15 observations of the main-on state. Due to the large number of distinct pulse shapes and due to the fact that they have a relatively low level of unpulsed flux, the positive flux criterion has led to an exclusion of about 90% of the whole parameter space of possible symmetry points Φ_1 and $\Phi_1 + \Delta$. Further sorting out the decompositions (i.e. the single-pole pulse profiles) that are qualitatively too complicated to match the criterion of two independent emission regions only left over one type of decomposition. The energy dependence of this type of decomposition is as smooth as that of the pulse profiles. Thus we have found acceptable decompositions in a small range of Φ_1 and $\Phi_1 + \Delta$ which are all of the same type. This type of decomposition is unique in the sense that a small deviation from the 'best-values' of the symmetry points results in decompositions that look similar but become more and more complicated the larger the deviation becomes until they do not match the physical criteria any more. A systematic variation of the best-values of the symmetry points, which could be caused by free precession of the neutron star, is not observed. The lower panels in Figure 2 show the decompositions of the typical pulse profiles of the respective top panels. The unpulsed flux has been distributed to the single-pole pulse profiles according to the constant C as derived in the second step of the analysis (see § 2.1). The single-pole pulse profiles show that the energy dependence of the pulse profiles is mainly due to the change of one polar contribution (dashed curve) where an additional peak appears above 10 keV, whereas the pulse shape of the other pole (solid curve) does not change much. Interestingly, the contributions of the emission regions we obtain look very similar to those of Panchenko & Postnov (1994) obtained from a model calculation mentioned in § 1. Similar components were also obtained by Kahabka (1987) in an attempt to model the observed pulse shapes by means of 3 to 5 gaussians, a sinusoidal component and a constant flux.

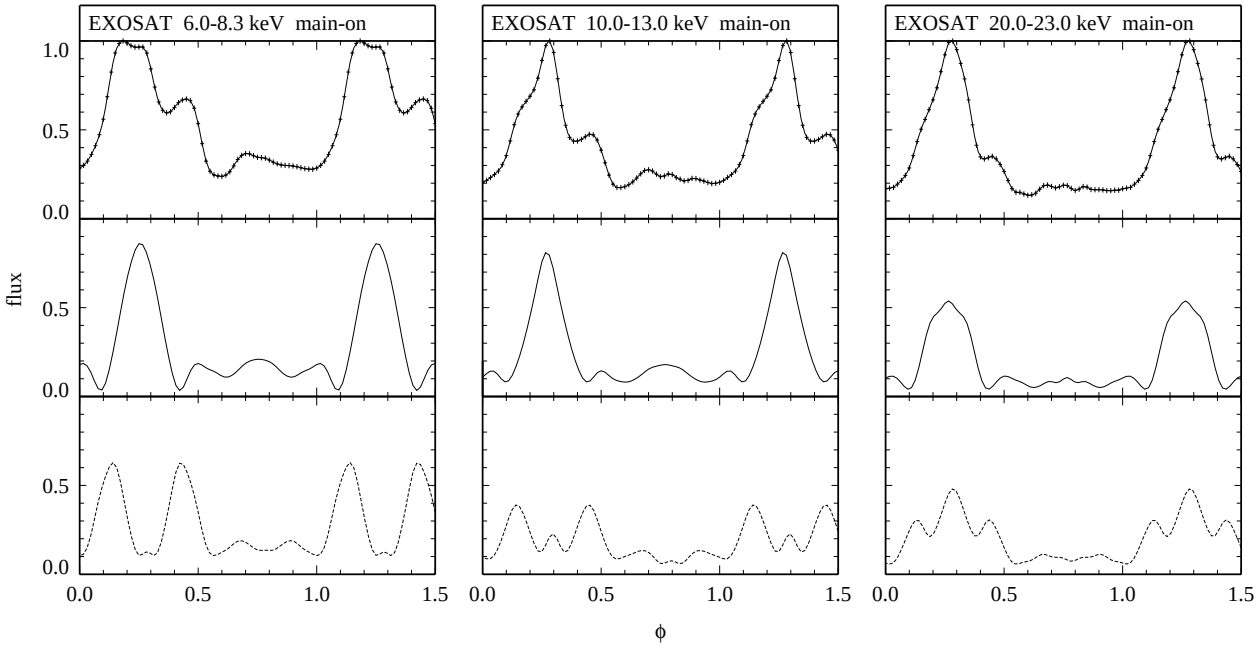

Fig. 2.— *Examples of analyzed pulse profiles and their decompositions into single-pole contributions. The panels in the top row show observed pulse profiles: the crosses correspond to the bin-width (60 phase bins) and the estimated statistical error of the observations, whereas the solid curves are the inverse Fourier-transformed pulse profiles using 32 Fourier coefficients. The pulse profiles have been normalized to have a maximum flux of unity. The energy range is indicated above each column. The energy dependence is typical for pulse profiles of the main-on state. The middle and bottom panels show the decompositions of the pulse profiles into the two symmetric contributions from the poles with symmetry points at* $\Phi_1 \approx 95^\circ$ *(*$\phi \approx 0.26$*) and* $\Phi_1 + \Delta$ *with* $\Delta \approx 9^\circ$ *(*$\phi \approx 0.29$*). The single-pole pulse profiles add up exactly to the pulse profile in the respective top panel.*

Extending the analysis to the short-on and the turn-on of the main-on we also find acceptable decompositions in the same range of the symmetry points as in the main-on. Since the pulses of the short-on state have quite a different shape compared to the main-on, their decompositions look different as well. An example of a typical short-on pulse profile and its decomposition is given in Figure 3.

b. search for an overlap region and determination of the geometry

In the next step of the analysis a two parameter fit has been applied to the decompositions in order to find out whether there is a range where the shapes of the polar contributions match. For the 62 pulse profiles of 8 of the main-on observations we have found a set of fit parameters which correspond to an overlap range where the two curves of each decomposition match astonishingly well if the statistical errors of the data are taken into account. This is shown in Figure 4 where the solid (dashed) curve corresponds to the respective single-pole pulse profile in Figure 2. The typical errors ($\pm\sigma$) as derived from error propagation of the statistical errors of the data are indicated in the upper right corner of each panel. The range where the curves overlap corresponds to values of the viewing angle θ under which both emission regions are seen during the course of one revolution of the neutron star. Introducing a scaling factor as an additional fit parameter we have achieved acceptable fits for the 15 pulse profiles of another three main-on observations. These profiles are further discussed in §3.2. No acceptable fits have been achieved for only four observations at late phases of the main-on when the flux had already dropped to less than 60% of the maximum flux of the respective 35-day cycle.

The dependence of the results for the location of the magnetic poles on the direction of observation Θ_O is shown in Figure 5. Assuming that Θ_O is equal to the inclination i of the system and adopting $i = 83°(\pm 4°)$ (Kunz 1996, private communication), we obtain the polar angles of the magnetic poles $\Theta_1 \approx 18°$ and $\Theta_2 \approx 159°$ with an offset from antipodal positions of $\delta < 5°$ (see Figure 1). The small value obtained for δ confirms the assumption that a fairly small distortion of the magnetic dipole field is enough to explain the considerable asymmetry of the pulse profiles of Her X-1. The error bars at $\Theta_O = 83° \pm 4°$ demonstrate how little the best fit-parameters determined for different pulse profiles vary.

The remaining ambiguity in the determination of the beam pattern is indicated by the different units of the lower (θ_+) and the upper (θ_-) x-axis in Figure 4. However as discussed in § 3.2 the study of the evolution of the pulse profile with the 35-day cycle indicates that the θ_+-solution is presumably the correct one. The beam pattern of the emission regions has been reconstructed in the range $66° < \theta_+ < 116°$ or $64° < \theta_- < 114°$ (for $\Theta_O = 83°$). The emission regions are unobservable under values of θ_+ (θ_-) outside this range.

Concerning the decompositions of the short-on pulse profiles, fits of a quality similar to those found for the main-on are not found. Additionally the values of the best fit parameters

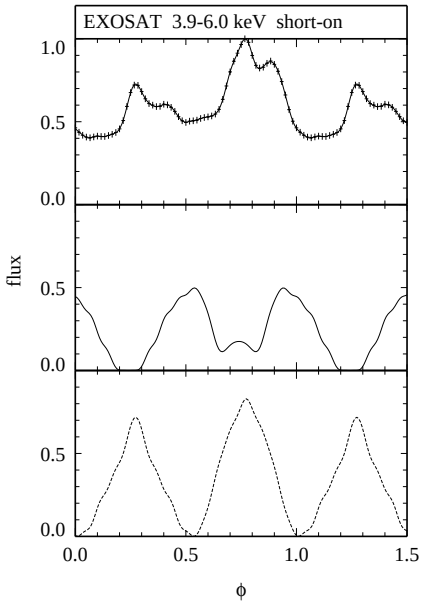

Fig. 3.— *Pulse profile of an EXOSAT observation (Kahabka 1987) during the short-on state and its decomposition. Plot symbols and normalization are as in Figure 2.*

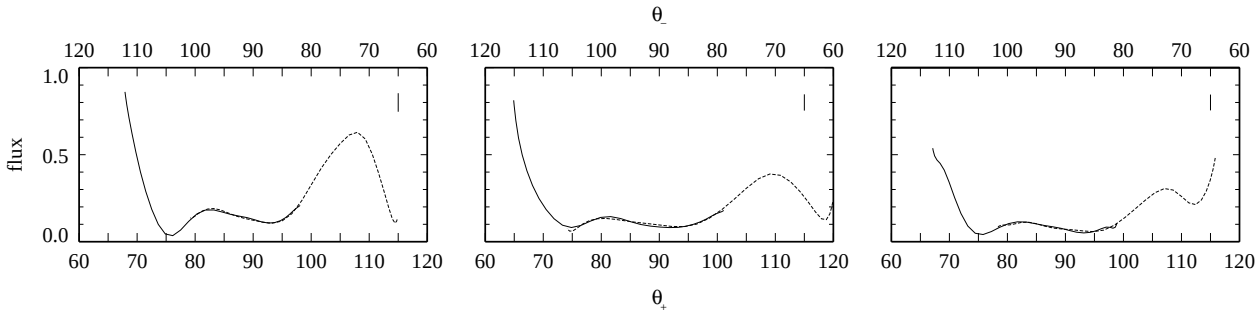

Fig. 4.— *Reconstructed beam patterns corresponding to the pulse profiles and their decompositions in Figure 2 as functions of the viewing angle θ between the local magnetic axis and the direction of observation. The θ_+- and the θ_--solutions correspond to the lower and upper x-axis respectively. The typical errors ($\pm\sigma$) are indicated in the upper right corner of each panel. The scale of the x-axis corresponds to $\Theta_O = 83°$.*

are different from each other and different from those of the main-on. The same holds true for the pulse profiles of the observation of the turn-on which unfortunately ended already when the flux had reached about 2/3 of the maximum flux of this 35-day cycle, as the lightcurve of the All-Sky-Monitor (ASM) onboard Rossi X-ray Timing Explorer (RXTE) shows (Wilms 1999, private communication).

3. Interpretation

The results show that the pulse profiles of Her X-1 are compatible with the idea that the beam pattern is symmetric and that a distorted dipole field is responsible for the asymmetry of the pulse profiles. The analysis does not permit to discriminate between exact symmetry and a small asymmetry of the beam pattern. In the case of a small asymmetry, test calculations suggest that the beam pattern derived above can be regarded as a fair approximation to the azimuthally averaged beam pattern. Considering the above results a large asymmetry of the beam pattern seems unlikely. A prominent asymmetry of the pulse profiles that is primarily due to an asymmetric beam pattern cannot in general be mimicked by displaced symmetric emission regions, because one choice of displacement will hardly produce simple and smooth 'false-symmetric constituents' for many different energies and luminosities with their respective distinct asymmetric pulse shapes. However, the possibility that the asymmetry of the pulse profiles of Her X-1 is primarily due to an asymmetric beam pattern cannot be rigorously excluded. With this caveat in mind, we will in this section discuss the consequences of the reconstructed symmetric beam pattern.

3.1. Beam Pattern

The beam pattern can also be plotted as a polar diagram with the magnetic axis ($\theta = 0°$) as symmetry axis. This is done in Figure 6. It shows the θ_+-solution for the beam pattern in the energy ranges 6.0 - 8.3 keV (solid line) and 20.0 - 23.0 keV (dashed line). In the overlap range the mean values of the single-pole contributions are plotted. Each beam pattern is normalized so that the total power emitted into the observable solid angle is unity. The θ_--solution can be obtained by turning the diagram upside down. No information on the beam pattern is available in the shaded regions.

The visibility of the emission region up to an angle of at least 116° is due to a lateral extension of the emission region along the neutron star surface, emission of radiation from the plasma at a certain height above the pole and relativistic light deflection near the neutron star surface. We can get an idea of the effect of light deflection if we imagine the emission to be originating from a hypothetical point source located at the pole of the neutron star. With an assumption about the ratio of the radius of the neutron star r_n to its Schwarzschild-radius r_s, the asymptotic angle θ

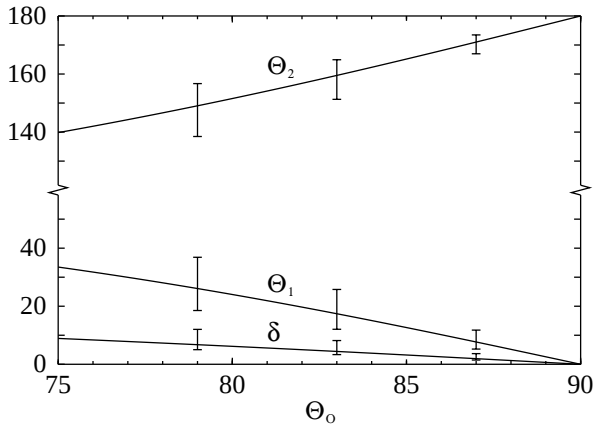

Fig. 5.— *Location of the magnetic poles in terms of their polar angles* Θ_1, Θ_2 *and their offset* δ *as described in Figure 1. The values determined for* Θ_1, Θ_2 *and* δ *depend on the viewing angle* Θ_O. *The curves for* Θ_1 *and* Θ_2 *are computed for the mean of the fit parameters a and b determined for each pulse profile individually. The curve for* δ *corresponds to the mean of the parameters a, b and* Δ. *Assuming that* Θ_O *is equal to the inclination i of the system, and adopting* $i = 83°$, *then* $\Theta_1 \approx 18°$, $\Theta_2 \approx 159°$ *and* $\delta < 5°$. *The curves determined for the parameters a, b and* Δ *for all pulse profiles individually lie within the error bars displayed at* $\Theta_O = i = 83° \pm 4°$.

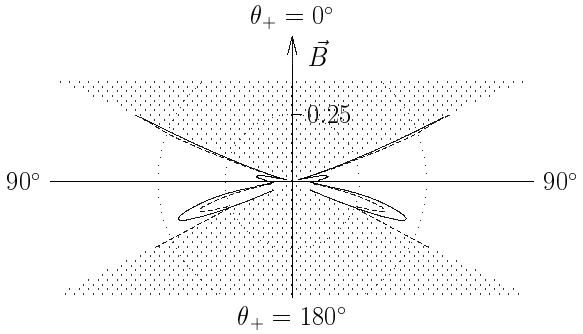

Fig. 6.— *Polar diagram of the beam patterns in the energy ranges 6.0 - 8.3 keV (solid) and 20.0 - 23.0 keV (dashed).* $\theta_+ = 0°$ *is the direction of the magnetic axis.*

under which the magnetic axis is seen by the distant observer can be transformed into the intrinsic angle ϑ under which the radiation is emitted from the point source (see Figure 7). Figure 8 shows how this transformation changes the asymptotic beam pattern of Figure 6 for $r_{\rm n}/r_{\rm s} = 2.8$. Again the emission pattern is normalized to have an integrated power of unity. It also illustrates the necessity of taking the effects of relativistic light deflection into account when modelling the emission regions, as has been previously pointed out by other authors (e.g. Nollert et al. 1989).

All beam patterns obtained from the various observations exhibit the same basic structure and energy dependence. Only the relative sizes of their substructures differ. The overall structure is quite complex as can be seen from the representative beam patterns in Figure 6. It has an increasing component towards the direction of the magnetic axis. Near the highest angles of the visible range the flux has a maximum at $\theta_+ \approx 108°$. These major components can be interpreted as a pencil- and a fan-beam respectively. The relative size of the fan-beam component decreases with increasing energy. Another relatively small feature occurs at $\theta_+ \approx 80°$. Above 15 keV the beam pattern has an additional increasing component at $\theta_+ > 114°$. This feature seems to become dominant above 28 keV and might therefore be responsible for the observed widening of the main peak of the pulse profile in this energy range (Soong 1990a, Kuster 1998, private communication). The occurrence of such a feature in this energy regime indicates a possible relation with electron cyclotron absorption at about 40 keV, favoured by many authors (e.g. Gruber et al. 1999). Unfortunately the energy resolution and the statistics of the data covering the range above 30 keV available to us and suitable for the analysis was not good enough to give an insight into this property of the beam pattern.

The beam patterns describe the flux as a function of viewing angle θ in the various energy ranges. The results can also be plotted as energy dependent spectra showing the flux depending on energy for various viewing angles. The left panel in Figure 9 shows 12 beam patterns in the energy range between 0.92 and 26.0 keV obtained from pulse profiles of an EXOSAT observation (Kahabka 1987). Since in the pulse profiles the response of the detectors is not considered, the flux of the beam patterns derived from the pulse profiles is normalized at the arbitrarily chosen angle $\theta_+ \approx 90°$ (indicated by an arrow). The angular range is divided into four sections in which the main features of the beam patterns are located. The other panels of Figure 9 show spectra at various viewing angles θ_+. Due to the normalization, the spectrum at the angle of normalization is just a horizontal line and all other spectra are relative to that particular one. Each spectrum contains two curves corresponding to the ME-Argon and the ME-Xenon proportional counters of EXOSAT. It can be easily seen that the spectra in section III, interpreted as fan-beam, are very soft compared to the spectra in section I, interpreted as pencil-beam. The spectra in section IV, interpreted as the high energy feature above, are even harder than those in section I. It should be pointed out that there is a great difference between the kind of spectra presented here and spectra obtained from pulse phase spectroscopy. At a particular pulse phase the poles are generally seen under different viewing angles and the spectra from both poles are always superposed. Nevertheless we can indentify the sections in the beam pattern that are responsible for features

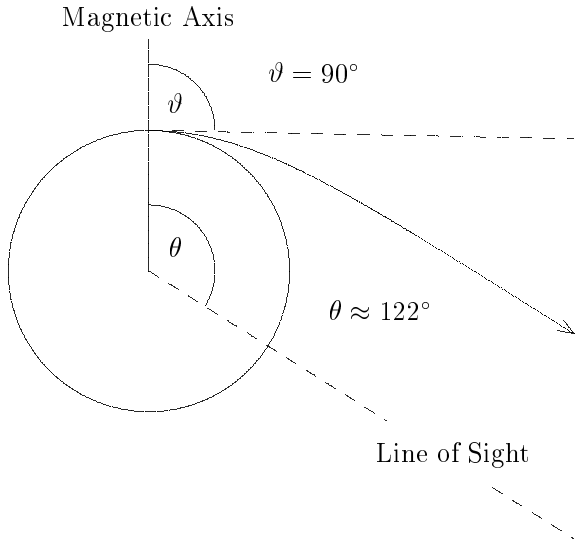

Fig. 7.— *Effect of light deflection on a photon that is emitted at the magnetic pole on the surface of a neutron star at the local angle* $\vartheta = 90°$ *with respect to the magnetic axis. An observer far away from the star observes the photon at a larger angle* θ*. The photon orbit shown in the figure has been calculated for a neutron star with* $r_n/r_s = 2.8$ *(e.g.* $M_n = 1.3\ M_\odot$ *and* $r_n = 10.64$ km*).*

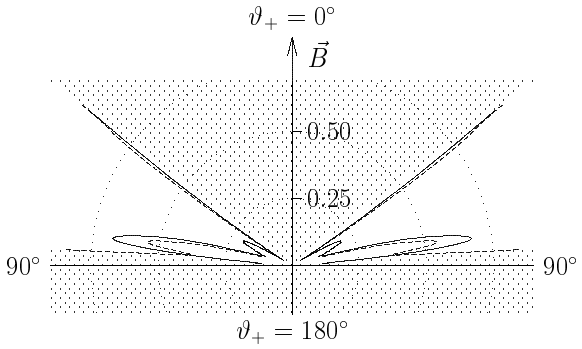

Fig. 8.— *Polar diagram of the intrinsic emission pattern of a hypothetical point source at the magnetic pole for* $r_{\rm n}/r_{\rm s} = 2.8$ *corresponding to the asymptotic beam patterns of Figure 6.*

in the pulse profile. Then we compare the spectra in these sections with spectra at the phases where the corresponding features in the pulse profile occur. E.g. section III of the beam pattern corresponds to the maxima of the second single-pole contribution around phases 0.15 and 0.45 (see Figure 2) which are responsible for the shoulder in the leading edge and the secondary maximum in the trailing edge of the peak of the pulse profile. The hardness ratio at these parts of the pulse profile is relatively low (see e.g. Deeter et al. 1998) which is consistent with the soft spectra in section III. On the other hand the hardness ratio at the peak of the pulse profile is very high corresponding to the sections I and IV where the spectra are relatively hard as well.

Due to the anisotropy of the beam pattern the flux depends on the viewing angle and therefore on the location of the poles and the inclination of the system. Then the observed luminosity of the pulsar also depends on the geometry and the inclination. Since we expect other pulsars to have similar anisotropic beam patterns but different geometries and inclinations, the fact that none has a luminosity $L_{\rm x} \gg 10^{38}$ erg/s indicates that the trend of the flux to increase towards the direction of the magnetic axis can be expected to reverse at small viewing angles. This would be consistent with the picture of the radiation escaping into the direction of the magnetic axis being blocked due to electron cyclotron absorption.

Since the components identified in the energy dependent beam pattern and the corresponding parts of the pulse profile directly reflect the properties of the processes of the emission regions, the beam pattern should be further compared with emission models.

3.2. Evolution of the Pulse Profile with the 35-day Cycle

The evolution of the pulse profile with the 35-day cycle has been studied intensively by many authors (e.g. Kahabka 1987, Ögelman & Trümper 1988, Soong et al. 1990b, Scott 1993). Deeter et al. (1998) summarize the observations establishing that the changes in pulse profile throughout the course of a 35-day cycle are systematic. Several attempts have been made to explain the change of the pulse shape with the 35-day phase (e.g. Bai 1981, Trümper et al. 1986, Petterson et al. 1991). In this section we discuss a scenario in which the column densities along the lines of sight onto the poles are different due to a partial obscuration of the neutron star by the inner edge of the accretion disk. This results in a different attenuation of the polar contributions.

As observed in a two day long continuous monitoring by RXTE, the pulse shape of Her X-1 does not change significantly during turn-on, whereas the spectra show strong photoelectric absorption (Kuster et al. 1998). This is in contrast to the behaviour during the decline of the main-on, when the pulse shape undergoes systematic changes while no spectral changes are prominent (Deeter et al. 1998, and references therein). The observations concerning the spectral behaviour can be explained in terms of a twisted and tilted accretion disk (Schandl & Meyer 1994). At turn-on the outer edge of the warped disk recedes from the line of sight to the neutron star whereas at the end of the main-on the inner edge sweeps into the line of sight. Since the

obscuring material at the outer edge of the disk is relatively cool compared to the very dense material at the inner edge, photoelectric absorption is only present during turn-on. By taking into account the scale heights of the corresponding parts of the disk, a warped disk profile also provides a mechanism to explain the different behaviour of the pulse shape. The density gradient in the obscuring material at the outer edge of the disk is relatively small. Thus the radiation emerging from both polar regions experiences the same absorption and the pulse profile does not change appreciably during the early stages of the main-on. Since on the other hand, the scale height of the inner edge of the disk is comparable to the size of the neutron star, the poles become obscured successively towards the end of the main-on. Therefore the radiation from one pole becomes attenuated more with respect to the other, leading to changes in the pulse profile. This situation is schematically illustrated in Figure 10. The different attenuation of the radiation from the poles is apparent in the decompositions. Figure 11 shows two pulse profiles of an EXOSAT observation (Kahabka 1987) during one 35-day cycle at $\Psi_{35} = 0.136$ near maximum intensity (solid) and at $\Psi_{35} = 0.234$ during the decay phase of the main-on state (dotted). The shoulder in the leading edge and the secondary maximum in the trailing edge of the peak are less prominent in the decay phase. We find that we can model the pulse profile at the end of the main-on state with the decompositions found for the pulse profile at maximum intensity by scaling one component with respect to the other. The pulse shape plotted with crosses in Figure 11 is reproduced from the decompositions of the pulse shape at maximum intensity by scaling the second component by a factor of 0.7 and adding the unscaled first component. It indeed closely resembles the features of the pulse profile in the decay phase. We conclude that during the decay phase the neutron star was partly obscured.

The fact that the second component has to be scaled simply means that the radiation from the second pole is attenuated more than the radiation from the first pole. Therefore the second pole must be located on that side of the neutron star which is on the opposite side of the accretion disk with respect to the observer. This enables us to decide between the θ_-- and the θ_+-solution discussed in section 2.3. It follows that the second component must correspond to the higher values of the viewing angle θ and therefore the θ_+-solution must be the correct one. In a previous analysis of pulse profiles of the X-ray binary Cen X-3 (Kraus et al. 1996), we have also found unique decompositions and the beam patterns and their energy dependence are quite similar to those of Her X-1. But we were not able to decide between the θ_+- and the θ_--solution. However the similarity of the beam patterns suggests that the θ_+-solution is the correct one for this pulsar, too.

Many authors have noted a narrowing of the main peak during the decay phase of the 35-day cycle (see Kunz 1996). Different attenuation of the components obtained in the analysis provides a natural explanation of this behaviour of the pulse profile.

As the amount of matter along the lines of sight increases, not only attenuation but also scattering of radiation from other directions into the line of sight increases. This leads to an

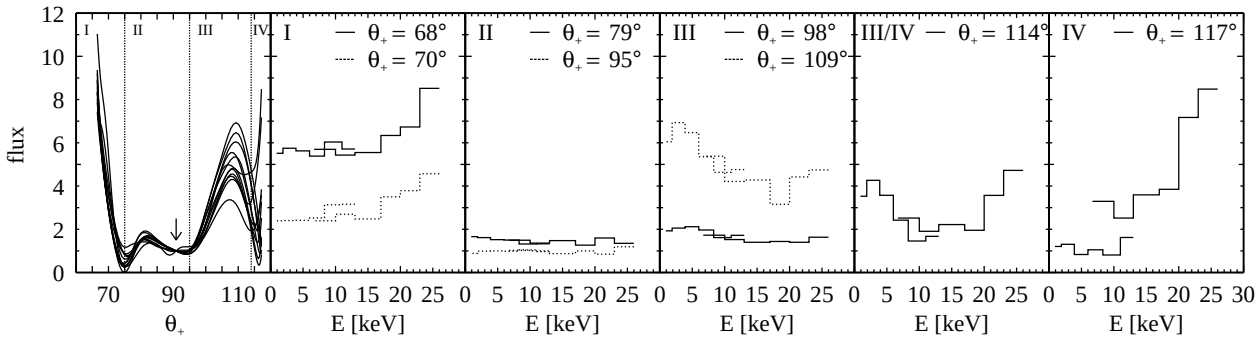

Fig. 9.— *Normalized beam patterns (left) and spectra at various viewing angles θ_+ obtained from the analysis of energy dependent pulse profiles of an EXOSAT observation. The normalization point $\theta_+ \approx 90°$ of the beam pattern is indicated by an arrow in the left panel. The range of the viewing angle has been divided into sections I-IV where the spectra differ. The two curves of each spectrum correspond to the ME-Argon and the ME-Xenon proportional counters of EXOSAT. The corresponding section and viewing angle of each spectrum is given at the top of each panel.*

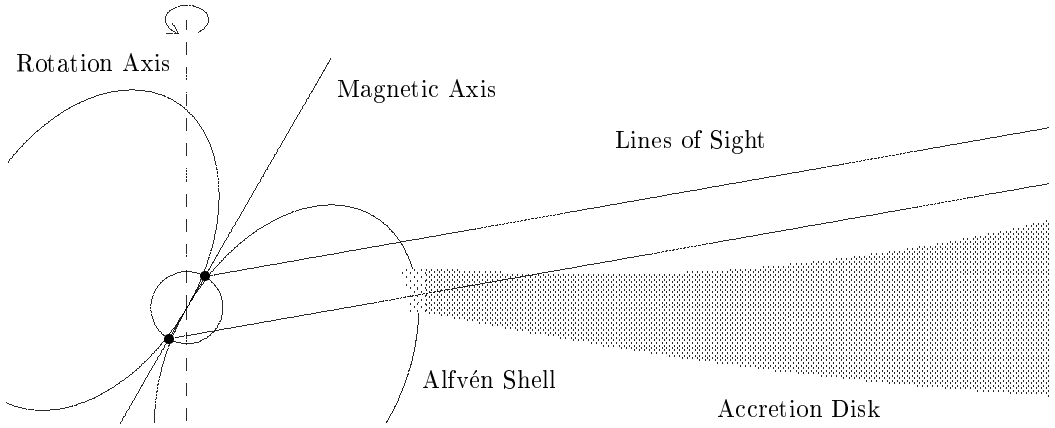

Fig. 10.— *Sketch of the situation during the decay phase of the 35-day cycle. The innermost part of the warped accretion disk intersects the line of sight onto the pole located on the far side of the disk with respect to the observer. Thus the radiation from that pole becomes significantly more attenuated than the radiation from the other pole. The scale height of the inner edge of the accretion disk is comparable to the size of the neutron star.*

increasing fraction of scattered flux in the pulse profile and the pulsed fraction [1] decreases. Other processes that lead to an increase of unpulsed flux are reprocessing of the direct beams by the interposed material or reflection from the disk (McCray et al. 1982). In other words the pulsed fraction is an indicator of the fraction of radiation that is coming directly from the polar regions. A pulse profile which contains a large fraction of scattered flux will have a small pulsed fraction. From such a pulse profile we can not expect to be able to reconstruct the beam pattern. Figure 12 shows that indeed the pulse profiles for which an acceptable fit has been found (denoted by filled symbols) are just those with a high pulsed fraction. The fact that the analysis of the pulse profiles of the short-on state has not led to acceptable fits can then be undestood in terms of the low value of their pulsed fraction. Accounting for possible attenuation, the components can be scaled in the fit procedure. This leads for the 15 pulse profiles of three main-on observations with a flux of about 70% of the typical maximum flux of the main-on state to a significant decrease of the deviation $\lambda^2_{\rm red}$ [2] between the two curves. These pulse profiles typically have a medium pulsed fraction.

Observations show that the spectral behaviour at X-ray turn-on is similar for the short-on and main-on states and that the pulse shape also changes during short-on (Deeter et al. 1998). This suggests that the configuration of the disk causing the spectral behaviour and the evolution of the pulse profile described above in the case of the main-on state is similar during short-on. Thus the outer part of the disk is responsible for the turn-on of the short-on state, whereas it ends when the inner edge of the disk passes into the line of sight.

This work has been supported by the Deutsche Forschungsgemeinschaft (DFG).

[1] pulsed fraction $= 1 - \frac{\text{minimum flux of pulse profile}}{\text{mean flux of pulse profile}}$

[2] $\lambda^2_{\rm red} = \frac{1}{N-\nu} \sum_{\rm N} (f_1({\rm i}) - f_2({\rm i}))^2$, where ν is the number of fit parameters

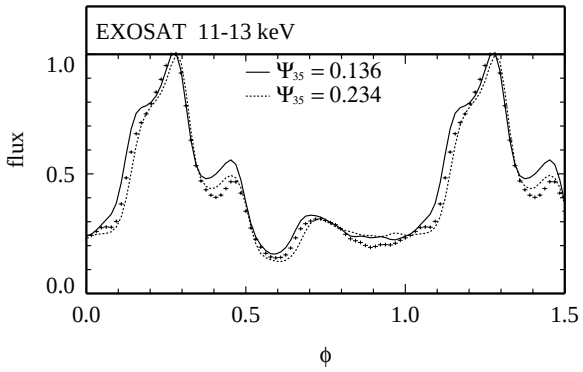

Fig. 11.— *Two pulse profiles of an EXOSAT observation within the same 35-day cycle during maximum intensity at* $\Psi_{35} = 0.136$ *(solid line) and during the decay phase at* $\Psi_{35} = 0.234$ *(dotted line). The crosses are a pulse profile reproduced from the decompositions of the maximum flux pulse profile with the contribution of the second pole being scaled by a factor of 0.7. It closely resembles the late phase pulse shape, especially in the main peak.*

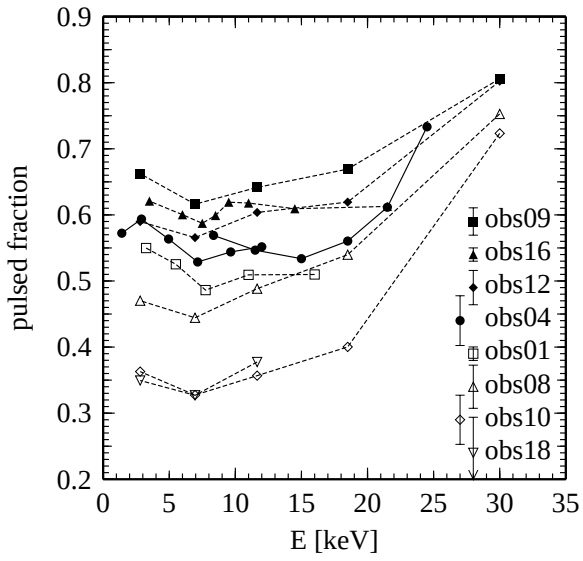

Fig. 12.— *Examples of the pulsed fraction vs energy for different observations. The filled symbols represent pulse profiles of the main-on state for which the beam pattern could be reconstructed. The pulse profiles corresponding to the open symbols are observations during the short-on (obs18), the decline phase of the main-on (obs10 and obs08) and during the rise-phase of the main-on (obs01) for which no overlap fit has been found. The typical errors indicated in the key for the different observations result from error propagation of the statistical errors of the pulse profiles. The pulsed fractions of each observation are connected with lines to guide the eyes. Note the minima of the pulsed fractions near 7 keV which are obviously due to non-pulsed iron line emission.*

REFERENCES

Bai, T. 1981, ApJ, 243, 244

Basko, M. M., & Sunyaev, R. A. 1975, A&A, 42, 311

Bildsten, L., Chakrabarty, D., Chiu, J., Finger, M. H., Koh, D. T., Nelson, R. W., Prince, T. A., Rubin, B. C., Scott, D. M., Stollberg, M., Vaughan, B. A., Wilson, C. A., and Wilson, R. B. 1997, ApJS, 113, 367

Deeter, J. E., Boynton P. E., and Pravdo, S. H. 1981, ApJ, 247, 1003

Deeter, J. E., Scott, D. M., Boynton, P. E., Miyamoto, S., Kitamoto, S., Takahama, S., and Nagase, F. 1998, ApJ, 502, 802

Gruber, D. E., Heindl, W. A., Rothschild, R. E., Staubert, R., Wilms, J., and Scott, D.M., 1999, in: "Highlights in X-Ray Astronomy in Honour of Joachim Tr"umper's 65 th birthday", eds. B. Aschenbach & M. J. Freyberg, MPE Report 272, 33

Kahabka, P. 1987, PhD thesis, TU München, MPE Report 204

Kraus, U., Blum, S., Schulte, J., Ruder, H. and Mészáros, P. 1996, ApJ, 467, 794

Kraus, U., Nollert, H.-P., Ruder, H. and Riffert, H. 1995, ApJ, 450, 763

Kunz, M. 1996, A&A, S120, 231

Kuster, M., Wilms, J., Blum, S., Staubert, R., Gruber, D., Rothschild, R., and Heindl, W. 1998, Astrophys. Lett. Comm., 38, 161

Leahy, D. A. 1991, MNRAS, 251, 203

Leahy, D. A., & Li, L. 1995, MNRAS, 277, 1177

McCray, R. A., Shull, J. M., Boynton, P. E., Deeter, J. E., Holt, S. S., and White, N. E. 1982, ApJ, 262, 301

Nollert, H.-P., Ruder, H., Herold, H., and Kraus, U. 1989, A&A, 208, 153

Ögelman, H., & Trümper, J. 1988, Mem. Soc. Astron. Italiana, 59, 169

Panchenko, I. E., & Postnov, K. A. 1994, A&A, 286, 497

Petterson, J. A., Rothschild, R. E., and Gruber, D. E. 1991, ApJ, 378, 696

Riffert, H., Nollert, H.-P., Kraus, U., and Ruder, H. 1993, ApJ, 406, 185

Schandl, S., & Meyer, F. 1994, A&A, 289, 149

Scott, D. M. 1993 PhD thesis, University of Washington

Soong, Y., Gruber, D. E., Peterson, L. E., and Rothschild, R. E. 1990a, ApJ, 348, 634

Soong, Y., Gruber, D. E., Peterson, L. E., and Rothschild, R. E. 1990b, ApJ, 348, 641

Tananbaum, H., Gursky, H., Kellog, E. M., Levinson, R., Schreier, E. and Giacconi, R. 1972, ApJ, 174, L143

Trümper, J., Kahabka, P., Ögelman, H., Pietsch, W., and Voges, W. 1986, ApJ, 300, L63

Trümper, J., Pietsch, W., Reppin, C., Voges, W., Staubert, R. and Kendziorra, E. 1978, ApJ, 219, L105

Wang, Y.-M., & Welter, G. L. 1981, A&A, 102, 97